Materials Today Advances 8 (2020) 100079

Contents lists available at ScienceDirect

Materials Today Advances

journal homepage: www.journals.elsevier.com/materials-today-advances/

Environment-dependent edge reconstruction of transition metal dichalcogenides: a global search

D. Li [a, b], F. Ding [b, c, *]

[a] State Key Lab of Superhard Materials, College of Physics, Jilin University, Changchun 130012, PR China
[b] Center for Multidimensional Carbon Materials, Institute for Basic Science (IBS), Ulsan 44919, Republic of Korea
[c] Department of Materials Science and Engineering, Ulsan National Institute of Science and Technology (UNIST), Ulsan 44919, Republic of Korea

ARTICLE INFO

Article history:
Received 11 February 2020
Received in revised form
1 May 2020
Accepted 1 May 2020
Available online 23 June 2020

Keywords:
Transition metal dichalcogenide
Molybdenum disulfide
Edge reconstruction
Particle swarm optimization algorithm
First-principles calculation

ABSTRACT

The properties of an edge of a transition metal dichalcogenide (TMDC) sensitively depend on its atomic structure; therefore, knowing the exact structure is a precondition for predicting the applications of TMDC, such as in catalysis. Although some edge reconstructions of TMDCs have been reported in previous studies, a global search of TMDC edge structures and calculations of their stabilities are still absent. Here, we propose an approach to explore all possible edge reconstructions of a monolayer TMDC by employing the particle swarm optimization algorithm and first-principles calculations. Taking the most studied TMDC material, MoS_2, as a representative, we have built a database of the edge structures of TMDCs. Including the five experimentally observed edges, the thirty-four most stable edges with various sulfur concentrations are predicted for the first time. The most stable edge structures of 1H−MoS_2 in different environments along both the armchair and zigzag directions have been predicted and agree well with experimental observations. A specific edge of 1H−MoS_2 in the database can be stabilized by modulating the chemical composition of the atoms, which offers an efficient way to tune the properties of TMDC nanostructures, such as TMDC quantum dots and/or nanoribbons.

1. Introduction

The family of transition metal dichalcogenide (TMDC) two-dimensional (2D) materials has experienced impressive advancements in the past 10 years because of their exotic chemical and physical properties and many potential applications [1–5]. Different from graphene and hexagonal boron nitride (hBN), TMDCs exhibit a combination of an atomically thin crystal structure, a direct and tunable small bandgap, high catalytic activity, and robust flexible mechanical properties, which enable many applications for which graphene and hBN cannot be used. Because of the mature technology of its synthesis, high stability, and robust electronic properties, molybdenum disulfide (MoS_2) is the most explored TMDC material [6,7]. For example, MoS_2 is one of the most efficient catalysts for the hydrogen evolution reaction (HER) and hydrodesulfurization of sulfur-rich hydrocarbon fuels [8]. In sharp contrast to the noble metal Pt, MoS_2 is an efficient, inexpensive, and earth-abundant electrocatalyst [9–13]. Unlike graphene, the excellent thermodynamic stability and direct bandgap of 1H−MoS_2 result in much higher potential for applications than the other phases of MoS_2 (1T phase and several derivatives of the 1T phase). Notably, the edge structures of 1H−MoS_2 heavily affect the physical and chemical properties of 2D 1H−MoS_2 and its derivatives, such as nanoribbons, nanotubes, and quantum dots [14–16]. Previous experiments indicated that the HER activity of MoS_2 arises mainly from active edges instead of unmodified basal planes [7]. Although the basal plane of 1H−MoS_2 with vacancies is also active for the HER [17], the edges of 1H−MoS_2 have obvious advantages in catalyzing the HER [18,19]. To improve the catalytic activity of 1H−MoS_2 edges, strategies such as cutting MoS_2 into nanostructures have been employed [6,20–27]. Although these strategies were proven efficient, the lack of an unambiguous understanding of the edge structures of 1H−MoS_2 is a major challenge for further improving the catalytic activity of 1H−MoS_2.

Experimentally, the Mo-rich edge structures of 1H−MoS_2 were often observed, mostly under high vacuum, by using high-resolution transmission electron microscopy. Some of these edges are bare Mo edges [28–31], and others are sulfur-passivated [11,30,32]. The Mo-rich edges of 1H−MoS_2 were identified as the

* Corresponding author.
E-mail address: f.ding@unist.ac.kr (F. Ding).

https://doi.org/10.1016/j.mtadv.2020.100079

active sites of catalysis [6–8,22]. As of now, the mechanisms for forming various Mo-rich edges of 1H–MoS_2 are still not clear.

In addition to the catalytic activity, the stability of the edges of 1H–MoS_2 can be used to determine the shapes of the most stable nanostructures of 1H–MoS_2 via Wulff construction. Experimentally, the observed shape of the 1H–MoS_2 flake varies from hexagon to triangle via intermediate truncated or multi-apex triangles with changing experimental conditions [33–35]. Although various edge structures of 1H–MoS_2 have been reported, they are mostly pristine edges or slightly modified edges obtained by adding or removing a certain number of S or Mo atoms [36–38]. A pristine edge of 1H–MoS_2, which can be generated by directly cutting 1H–MoS_2 along a specific direction, always has many unpaired electrons or dangling bonds and is therefore mostly energetically unstable and may undergo edge reconstruction to passivate these dangling bonds [39]. Therefore, uncovering the likely edge reconstruction of 1H–MoS_2 and exploring the edge reconstruction-induced exotic physical or chemical properties are crucial. Moreover, as a two element composite, the chemical environment or chemical composition of the edge could also dramatically change the edge structure. Therefore, how the edge configuration of 1H–MoS_2 evolves with the chemical environment is also unknown.

Here, we develop an approach to predict the edge reconstruction of monolayer TMDCs based on the particle swarm optimization algorithm (PSO) and first-principles calculations. A database of edge structures of TMDCs is built, and taking MoS_2 as a representative, we systematically investigate the edge reconstructions of 1H–MoS_2 under various chemical environments. Our calculations show that the edge of monolayer 1H–MoS_2 can be heavily reconstructed into many possible atomic structures and that the pristine edges are mostly less stable. Thirty-nine highly stable edges of 1H–MoS_2 with various sulfur concentrations are predicted in our calculations, and this study provides excellent explanations for previous experimental observations. Furthermore, the electronic properties of 1H–MoS_2 nanoribbons and nanoflakes are studied.

2. Methods

The calculations are performed within the density functional theory framework, carried out within the Vienna ab initio simulation package [40,41] using the projector augmented wave method [42]. The S $3s^2 3p^4$ electrons and Mo $4d^5 5s^1$ electrons are treated as valence electrons. For all calculations, the Perdew–Burke–Ernzerhof generalized gradient approximation exchange and correlation functional is used [40,43]. Convergence tests give a kinetic energy cutoff of 350 eV, with a grid of spacing of $2\pi \times 0.03$ $Å^{-1}$ for the electronic Brillouin zone integration in all phases. The geometries are regarded as optimized when the remanent Hellmann–Feynman forces on the ions are less than 0.01 eV/Å. We choose the energy of a single atom of bulk sulfur as the chemical potential zero point.

3. Results and discussion

Owing to the inherent lack of inversion symmetry and unique sandwich-like atom stacking modes of 1H–MoS_2, the edges of 1H–MoS_2 have more complex possibilities than those of highly symmetrized graphene and 2D h-BN [44–47]. Mimicking the edge configurations of 1H–MoS_2 is much more difficult compared with those of graphene and 2D h-BN. Here, we develop an approach to predict the edge structures of 2D materials based on PSO, which has excellent performance in exploring the potential energy surface of a material. The basic framework of edge structure prediction is based on the CALYPSO code [48,49], which has been confirmed to be very efficient in the structure prediction field [50,51]. We use frozen nanoribbon models as initial configurations and perform structure prediction for the edge part of the frozen nanoribbon models (Figs. S1–2). The detailed computational methods can be found in the Supporting Information. We use 1–2 unit cells to perform the edge structure prediction. An extensive structure search of the 1H–MoS_2 edges is performed. Various chemical stoichiometries (Mo_xS_y, x = 1–4 and y = 1–4 for the single cell; x = 1–6 and y = 1–6 for the double cell) at an edge are considered to fully explore the potential energy surface of the edge configuration space of 1H–MoS_2. For each composition, approximately 1,500 candidate structures are calculated in our global search of the 1H–MoS_2 edges (Fig. S3). In experiments, the concentrations of sulfur and molybdenum atoms are controlled by the precursors, which are usually evaporated sulfur powders and MoO_3 [34]. To simplify calculations, the binary parameter of the chemical composition is converted into a single sulfur concentration ($C_s = y-2x$). Therefore, the structural stabilities of the candidate edges with various compositions can be evaluated together under a single parameter (sulfur concentration).

To fully understand the edge reconstruction of 1H–MoS_2, the edge formation energy (Fig. S4) as a function of sulfur concentration is plotted in the form of a convex hull diagram. The convex hull diagram is a widely used criterion for judging the thermodynamic stability of materials. Here, we use it to find the most stable edges at various sulfur concentrations. For the Mo-terminated zigzag edge (ZZM), S-terminated zigzag edge (ZZS), and armchair edge (AC) edges (Fig. S2), the variation trends of the edge formation energy curves at $\mu_s = 0$ eV are very similar, as shown in Fig. 1(a–c). As the sulfur chemical composition increases, the edge formation energy generally decreases. The edge formation energy vs. sulfur concentration diagram of the ZZM edge has a larger descent rate than those of the ZZS and AC edges (Fig. 1(b)), indicating that ZZM edges have a better ability to reach the energy balance with increasing sulfur chemical composition. Interestingly, with increasing sulfur concentration, the variation trend of the edge formation energies exhibits an obvious odd-even effect, especially for the ZZS and AC edges (Fig. 1(a) and (c)). This can be easily understood because an edge with an even number of sulfur atoms can easily balance the dangling bonds, thus decreasing the edge formation energy. Similar odd-even effects have been observed in the formation of sulfur dimer vacancies [52] and magnetic properties of MoS_2 [53]. The structural evolution with changing sulfur concentration (Fig. 2) also confirms this odd-even effect. For sulfur-rich situations, the sulfur atoms tend to form S_2-dimer-like units at an edge of 1H–MoS_2. Moreover, when μ_s is 0 eV, the most stable ZZM and AC edges are obviously located at $C_s = 4$, indicating that the ZZM and AC edges with sufficient sulfur concentrations are stable in sulfur-rich situations. However, for the ZZS edge, even if more sulfur atoms or metal atoms are added, the pristine sulfur-terminated zigzag edge is still the most stable edge at $\mu_s = 0$ eV. This result is in good agreement with experimental observations that the pristine sulfur-terminated zigzag edge is the most observed sulfur-terminated zigzag edge [33].

The most stable edge structures of the ZZS, ZZM, and AC edges at various sulfur concentrations are selected to construct the first database of 1H–MoS_2, as shown in Fig. 2 (Figs. S5 and S6). In addition to the five experimentally observed edges, 34 edges of 1H–MoS_2 are predicted for the first time. In perfect 1H–MoS_2, one Mo atom bonds with six S atoms, and one S atom bonds with three Mo atoms, forming a highly stable honeycomb lattice. However, in a nanoribbon or other finite nanostructure of MoS_2, the Mo atoms and S atoms at an edge no longer have perfect triangular prismatic coordination and triangular pyramidal coordination, respectively. Therefore, the pristine edges of 1H–MoS_2 usually have very high potential for reconstruction because of the presence of dangling bonds induced by excess unpaired electrons. These excess unpaired

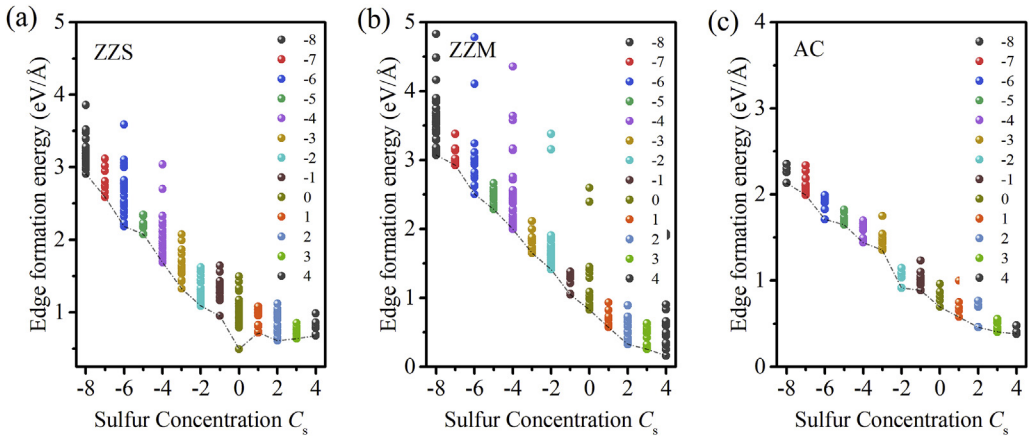

Fig. 1. Edge formation energies of the (a) S-terminated zigzag edge (ZZS), (b) Mo-terminated zigzag edge (ZZM), and (c) armchair edge (AC) as a function of sulfur concentration C_s at the chemical potential of sulfur $\mu_s = 0$ eV. The energy of bulk sulfur is selected as the zero point of the chemical potential.

electrons redistribute to ensure the energy balance of the system. When the sulfur concentration is 0, the pristine ZZS and ZZM edges are the most stable edges. However, the pristine AC edge undergoes a reconstruction to the AC_0 edge. Overall, the pristine ZZM, ZZS, and AC edges of 1H—MoS_2 tend to be covered by additional sulfur or metal atoms. The numbers of additional sulfur or metal atoms are determined by the sulfur composition. A common feature of edge reconstruction under sulfur-rich conditions is the occurrence of sulfur atom dimerization. S_2-dimer-like units frequently appear at the three types of 1H—MoS_2 edges, especially for the ZZM and ZZS edges. For the pristine ZZS edge, the coordination number of sulfur atoms at an edge is two. These unsaturated sulfur atoms need to bond with other atoms to balance their dangling bonds. When C_s is in the range of 0—4, the unsaturated sulfur atoms bind with S_2-dimer units or a mixture of metal atoms and S_2-dimer units. When C_s is in the range of −8 to 0, a combination of metal atoms and sulfur monomers instead of S_2-dimer units balances the dangling bonds of unsaturated sulfur atoms. For the pristine ZZM edge, the metal atoms at the edge have redundant electrons. The redundant electrons of metal atoms at the edge will redistribute. When C_s is 4, two pairs of S_2-dimer-like units bond with metal atoms at the edge. These two pairs of S_2-dimer units are parallel to each other. As C_s decreases, the two pairs of S_2-dimer units transform into a mixture of a S_2-dimer unit and sulfur monomers and finally into sulfur monomers. When the metal-rich situation is reached, metal atoms at an edge are covered by a combination of metal and sulfur atoms. For the pristine AC edge, S_2-dimer units and sulfur monomers appear at the edge when C_s is in the range of 2—4. When C_s is less than 2, a combination of metal and sulfur atoms covers the pristine AC edge. In our calculations, the metal-rich edges with 'Mo dimer' units are not energetically favorable with respect to the sulfur-terminated metal-rich edges. Therefore, the experimentally observed bare 'Mo dimer' edge is a sulfur-terminated edge because the sulfur atoms are usually not easy to distinguish in the scanning transmission electron microscopy (STEM) images, or the sulfur atoms are knocked out by electron irradiation.

The chemical potential is another important factor for the stability of edge structures in addition to the thermodynamic stability. To simultaneously investigate the effect of the chemical potential and chemical composition on the 1H—MoS_2 edge, we plot the edge formation energy vs. chemical potential and chemical composition curves in Fig. 3(a—c). According to previous theoretical and experimental studies [37,38], the chemical potential of sulfur is chosen in the range of −1.5 eV—0.5 eV, which is relative to the energy of bulk sulfur. Both sulfur-rich and metal-rich situations are considered in our calculation. With changing chemical potential of sulfur, the variation trends of the edge formation energies for the ZZS, ZZM, and AC edges are very similar. Several local minima are observed in the edge formation energy curves, especially for the ZZS and AC edges. However, the intersection points of the edge formation energies for the ZZS, ZZM, and AC edges under various chemical potentials are different because of the intrinsic

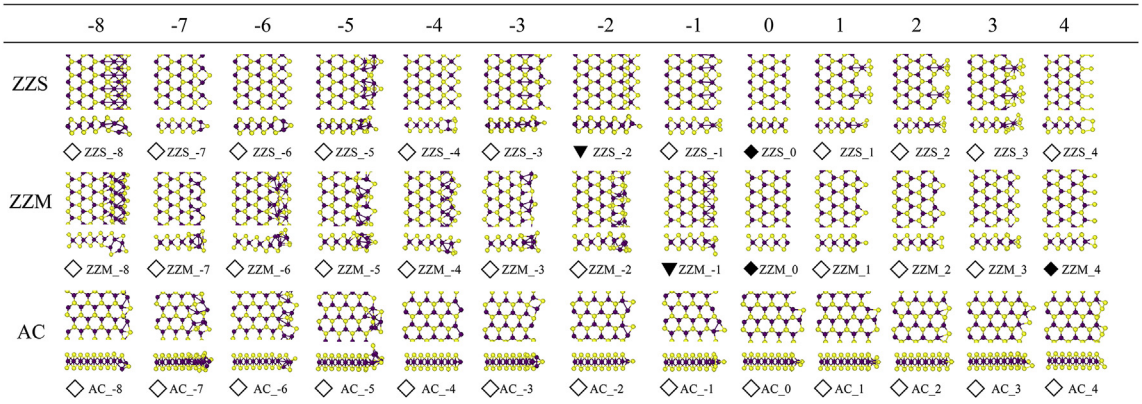

Fig. 2. Top and side views of the most stable edge structures of the ZZS, ZZM, and AC edges at various sulfur concentrations. The ◊, ▼ and ◆ shapes indicate the edges found in the current work only, in previous experiments, and in previous theoretical and experimental works, respectively. ZZS, S-terminated zigzag edge; ZZM, Mo-terminated zigzag edge; AC, armchair edge.

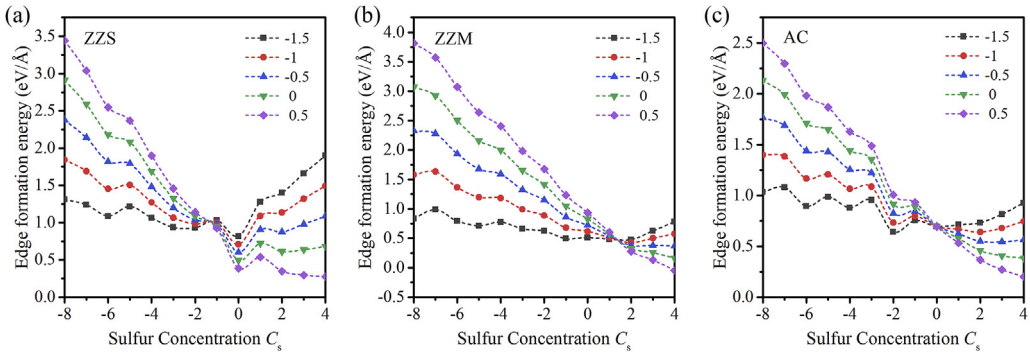

Fig. 3. Variation in the edge formation energy of 1H−MoS_2 as a function of chemical potential and chemical composition. ZZS, S-terminated zigzag edge; ZZM, Mo-terminated zigzag edge; AC, armchair edge.

differences in the chemical bonding environment of the initial pristine edges. For ZZS edges, the intersection point of edge formation energies is close to the value of −1 because the initial pristine ZZS edge is a metal-deficient edge (Fig. 3(a)). The sulfur atom bonds at the edge of the initial pristine zigzag edge are unsaturated. These atoms need to bond with metal atoms to balance the dangling bonds. In contrast to ZZS edges, the initial pristine ZZM edge is a sulfur-deficient edge. The intersection point of edge formation energies is close to the value of 1 for ZZM edges because the metal atoms at the edge need sulfur atoms to balance their dangling bonds (Fig. 3(b)). For AC edges, the intersection point of edge formation energies is located at zero because the initial pristine AC edge is not affected by the chemical potential (Fig. 3(c)). Interestingly, the odd-even effect of edge formation energies is enhanced by a decrease in the chemical potential of sulfur, especially for AC edges.

For ZZS edges (Fig. 3(a)), under an extremely high chemical potential of sulfur, the most stable edge structure is located at $C_s = 4$. As the chemical potential of sulfur decreases, a small energy barrier at $C_s = 1$ is crossed at $\mu_s = 0$ eV. The ZZS_0 edge gradually becomes the most stable edge structure when μ_s is in the range of 0 to −1.5 eV. The pristine ZZS edge (ZZS_0) is very special because it is almost the most stable edge over the whole range of chemical potential μ_s. Under the metal-rich situation, two local minima occur when C_s is in the range of −2 to −6 (ZZS_-2 edge and ZZS_-6 edge). However, the edge formation energies of the ZZS_-2 edge and ZZS_-6 edge are still higher than that of the initial ZZS_0 edge. In total, four local minima occur over the whole range of μ_s. The energy differences between the ZZS_0 edge and ZZS_-2/ZZS_-3 edge decrease with decreasing μ_s. At $\mu_s = -1.5$ eV, the energy difference between the ZZS_0 edge and the ZZS_-2/ZZS_-3 edge is approximately 0.12 eV/Å, which can be easily overcome at high temperatures. The metastable ZZS_-2 edge and ZZS_-3 edge are expected to appear in experiments. Similar edge structures have been observed in experiments, which were denoted the DT edge and Mo-Klein edge (Fig. S7). We calculated the edge formation energies of our proposed and experimentally observed edges as shown in Fig. 4(a) and compared the structural features of them with the experimental observations (Fig. 4(b–d)). The ZZS_-2 edge can explain the STEM results of experiments [29]. The calculated edge formation energies indicate that the ZZS_-2 edge is more stable than the DT edge (Fig. 4(a)). Furthermore, the ZZS_-2 edge can also be used to explain Chen's experimental observations. The ZZS_-2 edge has a great advantage in energy compared with the Mo-replaced S edge. We also find that the metastable ZZS_-3_n2 edge (Fig. S5) in our database can explain the experimental STEM results very well (Fig. 4(b)). Although the ZZS_-3_n2 edge is the second most stable phase at $C_s = -3$, the edge formation energy of the ZZS_-3_n2 edge is much lower than that of the previously proposed Mo-Klein edge. Another local minimum edge, ZZS_-6, is expected to be stable at a lower μ_s.

For ZZM edges (Fig. 3(b)), the most stable structure is the ZZM_4 edge under high μ_s. This result is in good agreement with the previous study. The ZZM_4 edge is seen as the most stable structure in most studies [8,39,54]. As μ_s decreases, a very small energy difference at $C_s = 3$ is crossed. Then, the ZZM_2 edge becomes the most stable edge. According to Fig. 2, the outermost Mo atoms of the ZZM_2 edge and ZZM_4 edge are terminated by S_2-dimer-like units. At $\mu_s = -0.5$ eV, the energy difference between the ZZM_3 edge and ZZM_2/ZZM_4 edge is very small, indicating that they have almost equal chances of appearing in experiments. The ZZM_3 edge is alternately composed of S_2-dimer-like units and S monomers. At $\mu_s = -1.5$ eV, the energy differences among the ZZM_2, ZZM_1, ZZM_0, and ZZM_-1 edges are very small, indicating that they also have almost equal chances of appearing in experiments. The metal-rich ZZM_-1 edge has already been observed in recent experiments (Fig. 4(d)) [30,31]. Comparing edge formation energies (Fig. 4(a)), the ZZM_-1 edge is energetically more favorable than the candidate structure proposed by Zhou et al. [30,31] Furthermore, we found that Mo atoms at an edge are passivated by sulfur atoms even if the metal-rich situation is reached. The edges with bare Mo atoms do not have an advantage in energy. The reason for the experimentally observed bare Mo edges should be that the electron irradiation knocks out the outermost sulfur atoms in experiments. Although the highly stable edges such as ZZM_-1, ZZS_-2, and ZZS_-3_n2 are not observed in experiments, they are very important for the deep understanding of edge reconstruction of TMDCs.

For AC edges (Fig. 3(c)), under extremely high chemical potential μ_s, the most stable edge structure is the sulfur-rich AC_4 edge. As μ_s decreases, the AC_4, AC_3, and AC_2 edges gradually become the most stable edges. When μ_s is extremely low ($\mu_s = -1.5$ eV), a small energy difference at $C_s = -1$ is overcome, and then, the AC_-2 edge becomes the most stable edge. The AC_-2 edge is also the global minimum of the potential energy surface at $\mu_s = -1.5$ eV. For the metal-rich situation ($C_s = -8 \sim -2$), as μ_s decreases, the odd-even effect of the edge formation energies of AR edges becomes more obvious. The edge formation energies exhibit an interesting periodic oscillation with changing C_s. However, the AC_-2 edge is still the global minimum, which is not affected by the odd-even effect-induced energy oscillation. Furthermore, under low μ_s, the energy difference between the most stable AC_-2 edge and the second most stable AC_-4 edge is approximately 0.24 eV/Å, indicating that a transition from the AC_-2 edge to the metal-rich edges (AC_-8, AC_-7, AC_-6, AC_-5, AC_-4, and AC_-3 edges) is very difficult even if more metal atoms are added. For the high μ_s situation, the energy difference between the most stable AC_-2 edge and sulfur-rich

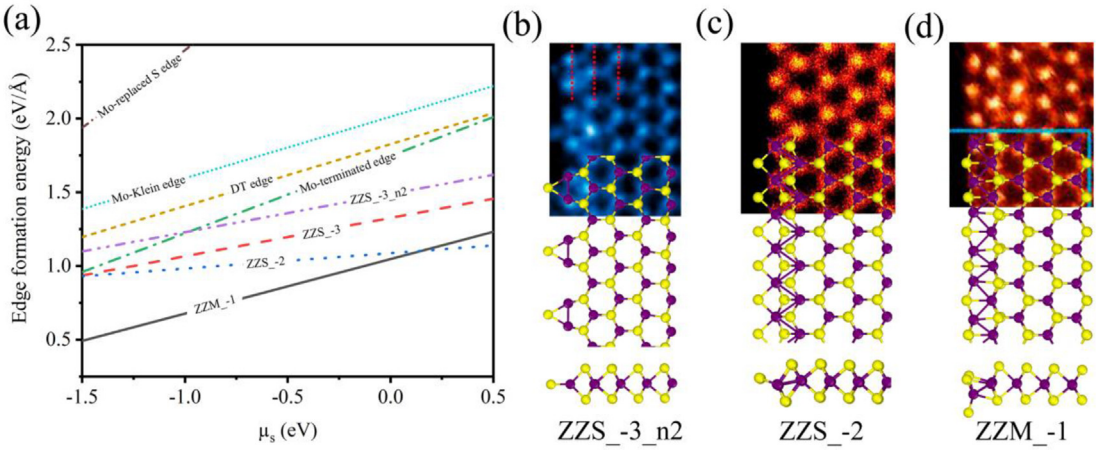

Fig. 4. (a) Edge formation energy as a function of chemical potential for selected edges. Comparison of experimental STEM observations and theoretical results of (b) ZZS_-3_n2, (c) ZZS_-2, and (d) ZZM_-1 edges. Reprinted (adapted) with permission from ref. 29 and ref. 30 Copyright 2013 and 2018 American Chemical Society. ZZS, S-terminated zigzag edge; ZZM, Mo-terminated zigzag edge.

edges (AC_-1, AC_0, AC_1, and AC_2 edges) is less than 0.1 eV/Å, and the edge formation energies of the AC_-1, AC_0, AC_1, and AC_2 edges are almost equal, suggesting that these sulfur-rich edges (AC_-1, AC_0, AC_1, and AC_2 edges) have equal possibilities of appearing in experiments.

We also investigated the relationship between the edge formation energies and the chemical potential of the ZZM, ZZS, and AC edges (Fig. 5). For ZZS edges (Fig. 5(a)), the ZZS_4 edge is the most stable edge when μ_S is in the range of 0.3−0.5 eV. ZZS_0 becomes the most stable when μ_S is less than 0.3 eV. As μ_S decreases, the ZZS_-3 edge and ZZS_-6 edge become more stable at μ_S of −1.75 eV and −1.82 eV, respectively. For ZZM edges (Fig. 5(b)), the ZZM_4 edge and ZZM_2 edge are the two most stable edges when μ_S is greater than −1.53 eV. The ZZM_4 edge transforms into the ZZM_2 edge at $\mu_S = -0.52$ eV. When μ_S is less than −1.53 eV, the ZZM_-1 edge and ZZM_-8 edge become more stable. The ZZM_-1 edge transforms into the ZZM_-8 edge at $\mu_S = -1.80$ eV. For AC edges (Fig. 5(c)), as μ_S decreases, the transition sequence is the AC_4, AC_3, AC_2, and AC_-2 edges. Overall, the reconstructed ZZM edges are always the most stable (Fig. 5(d)). For a high μ_S situation, the edge formation energy differences between ZZM edges and ZZS edges is greater than 0.4 eV/Å. As μ_S decreases, the energy difference between ZZM edges and ZZS edges decreases and becomes close to 0.2 eV/Å when μ_S is approximately −0.52 eV. Then, the

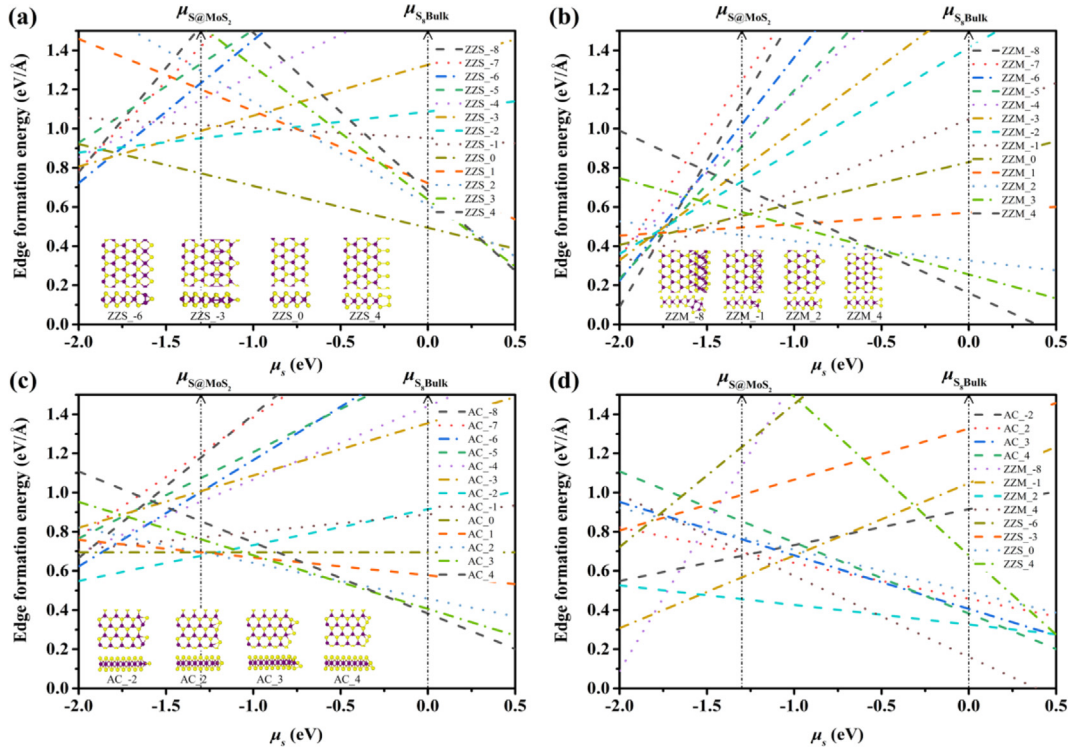

Fig. 5. Edge formation energies at various sulfur concentrations as a function of chemical potential μ_S for the (a) ZZS edge, (b) ZZM edge, and (c) AC edge. (d) Edge formation energies of the most stable edges of the ZZS, ZZM, and AC edges as a function of chemical potential μ_S. The structures of the most stable ZZS, ZZM, and AC edges are shown in the inset. ZZS, S-terminated zigzag edge; ZZM, Mo-terminated zigzag edge; AC, armchair edge.

energy difference between ZZM and ZZS edges increases again. The variation trend of the energy difference between ZZS and AC edges is similar to that between ZZM and ZZS edges. The energy difference between ZZS and AC edges is greater than 0.12 eV/Å under a high chemical potential of sulfur. As μ_S decreases, the energy difference between ZZS and AC edges becomes small. When μ_S is in the range of −1.265 eV to −0.05 eV, the energy difference remains at approximately 0.1 eV/Å. When μ_S is less than −1.26 eV, the energy difference between ZZS and AC edges increases again. At $\mu_S = -1.74$ eV, the energy difference between ZZS and AC edges is close to 0.26 eV/Å. As μ_S decreases, the energy difference between ZZS and AC edges decreases again. At $\mu_S = -2$ eV, the energy difference between ZZS and AC edges is approximately 0.18 eV/Å. The energy range of AC edges is located in the middle of the energies of ZZM and ZZS edges. AC edges will appear at a lower chemical potential of sulfur. Based on crystal growth theory, the edges with the lowest edge formation energy will be easily retained, and the edges with higher edge formation energies will disappear during growth. Therefore, the ZZM_4 edge can be easily obtained under high μ_S. The ZZM_2 edge can be obtained under low μ_S. At extremely low μ_S, the ZZM_-1 edge and ZZM_-8 edge will appear in experiments. The pristine ZZM edge is not stable because the dangling bonds of metal atoms need to be passivated.

Next, we study the electronic band structures of highly stable 1H−MoS_2 nanoribbons composed of the most stable edge structures at various chemical potentials (Fig. 6). Based on the analysis of the thermodynamic stabilities of 1H−MoS_2 edges (Fig. 5(d)), five highly stable zigzag nanoribbons (ZZ-NR-1, ZZ-NR-2, ZZ-NR-3, ZZ-NR-4, and ZZ-NR-5) and four highly stable armchair nanoribbons (AC-NR-1, AC-NR-2, AC-NR-3, and AC-NR-4) are constructed. A zigzag nanoribbon (ZZ-NR-0) composed of pristine ZZS and ZZM edges is considered as a reference. Our calculations indicate that ZZ-NR-0 is metallic (Fig. 6(a)). Both the S_*p* and Mo_*d* electrons contribute to the metallization of ZZ-NR-0. The five highly stable zigzag nanoribbons of 1H−MoS_2 are all metallic (Fig. 6(b–f)). This result is in good agreement with a previous study that reported that the zigzag edges of typical 2D semiconducting materials exhibit metallic properties [29]. However, the contributions of the S_*p* and Mo_*d* electrons to the metallization of the five highly stable zigzag nanoribbons of 1H−MoS_2 greatly differ with changing chemical potential of sulfur. A previous study confirmed that the electronic bands around the Fermi level in 2D TMDCs are mainly dominated by the edge atoms [55]. According to the projected band structures, under high μ_S, the metallic properties of zigzag nanoribbons are determined by both the *p* orbital of S atoms and *d* orbital of Mo atoms (Fig. 6(d–f)). Under low μ_S, the metallic properties are determined only by the *d* orbital of Mo atoms (Fig. 6(b and c)). These results provide a strategy to tune the catalytic activity of the edges of 1H−MoS_2 by changing the chemical potential of sulfur. Moreover, the four highly stable armchair nanoribbons of 1H−MoS_2 (AC-NR-1, AC-NR-2, AC-NR-3, and AC-NR-4) are semiconductors with obviously tunable bandgaps in the range of 0.4–1 eV (Fig. 6(g–j)). The obvious difference in the electronic properties between the zigzag and armchair nanoribbons of 1H−MoS_2 indicate that this material has potential applications in the catalysis and electronic device fields.

Fig. 7(a–j) shows the evolution of the equilibrium shape of 1H−MoS_2 nanoflakes with changing chemical potential of sulfur. Under high μ_S, the equilibrium shape of the 1H−MoS_2 nanoflake is a triangle with three ZZM_4 edges (Fig. 7(j)). This triangle can be maintained for μ_S in the range of 0.35 to −0.4 eV (Fig. 7(i and j)). As μ_S decreases, the vertex of the triangle exhibits some truncation. At $\mu_S = -0.4$ eV, the triangle transforms into a truncated triangle, which has a mixture of ZZS_0 edges and arbitrary chiral edges (Fig. 7(h)). As μ_S further decreases, the three ZZS_0 edges of the truncated triangle gradually first expand. When μ_S is less than −0.6 eV, the three ZZS_0 edges of the truncated triangle gradually shrink (Fig. 7(d–g)). At the same time, the AC_2 edge and AC_-2 edge have an obvious advantage in energy. They expand with decreasing μ_S. Finally, the 1H−MoS_2 nanoflake has a nonagonal shape with three ZZM_2 edges and six AC_-2 edges (Fig. 7(c)). A similar nonagonal shape was predicted in a recent study of monolayer GaSe nanoflakes [55]. When μ_S is extremely low, the nonagonal shape gradually reverts to the triangle (Fig. 7(a) and (b)). The triangular 1H−MoS_2 nanoflake composed of ZZM_-8 edges is the most stable shape at extremely low μ_S. Our simulations indicate that the shape of the MoS_2 nanoflake is strongly dependent on the chemical potential of sulfur, which induces the shape of the 1H−MoS_2 nanoflake to transform from a triangle to a truncated triangle and then back to a triangle. This result is in good agreement with previous theoretical calculations [56]. However, there are some differences in the equilibrium shape of 1H−MoS_2 nanoflakes

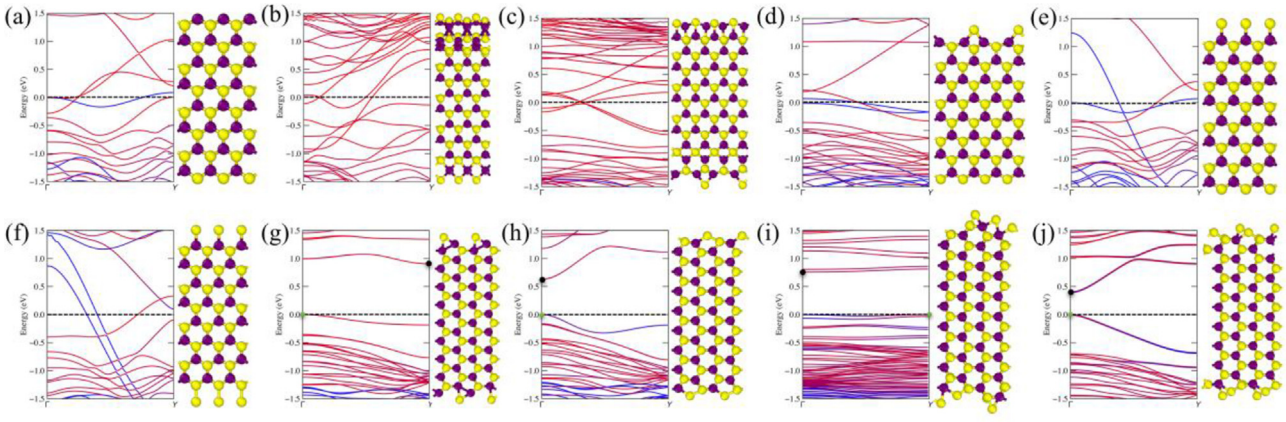

Fig. 6. Projected band structures of some highly stable MoS_2 nanoribbons. (a) A zigzag nanoribbon with pristine ZZM and ZZS edges (ZZ-NR-0), (b) a zigzag nanoribbon with ZZM_-8 and ZZS_-6 edges (ZZ-NR-1), (c) a zigzag nanoribbon with ZZM_-1 and ZZS_-3 edges (ZZ-NR-2), (d) a zigzag nanoribbon with ZZM_2 and ZZS_0 edges (ZZ-NR-3), (e) a zigzag nanoribbon with ZZM_4 and ZZS_0 edges (ZZ-NR-4), (f) a zigzag nanoribbon with ZZM_4 and ZZS_4 edges (ZZ-NR-5), (g) an armchair nanoribbon with two AC_-2 edges (AC-NR-1), (h) an armchair nanoribbon with two AC_2 edges (AC-NR-2), (i) an armchair nanoribbon with two AC_3 edges (AC-NR-3), and (j) an armchair nanoribbon with two AC_4 edges (AC-NR-4). The blue and red colors indicate the contributions of S_*p* and Mo_*d* electrons. The horizontal dashed lines denote the position of the Fermi level. The black and green spheres denote the positions of the lowest unoccupied molecular orbital (LUMO) and the highest occupied molecular orbital (HOMO), respectively. ZZS, S-terminated zigzag edge; ZZM, Mo-terminated zigzag edge; AC, armchair edge. (For interpretation of the references to color in this figure legend, the reader is referred to the Web version of this article.)

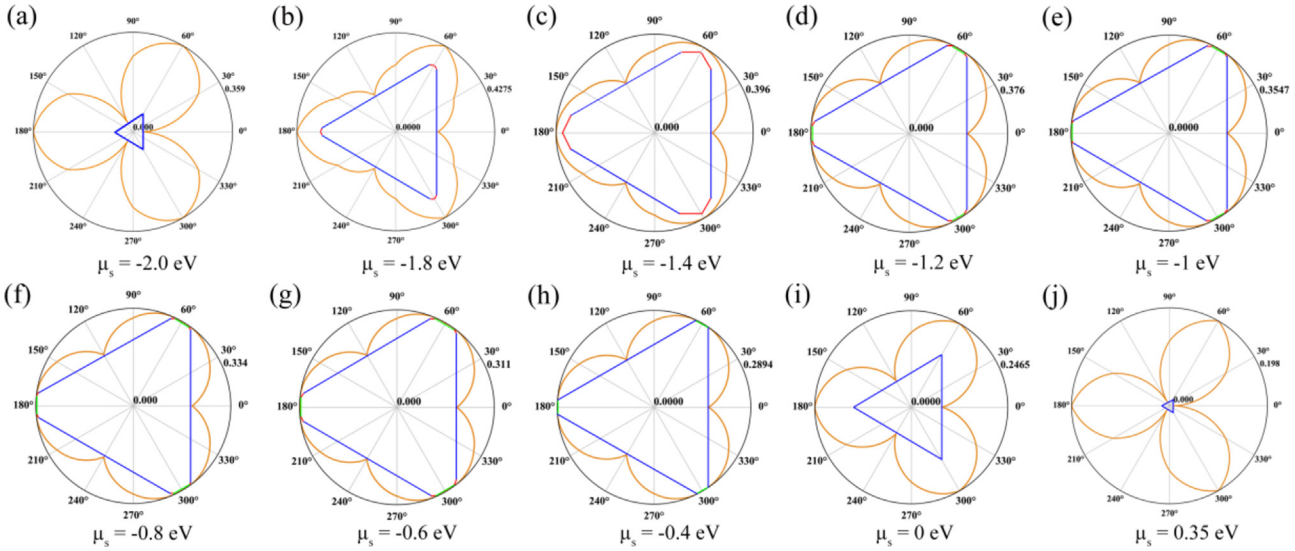

Fig. 7. Polar plots of the formation energies of MoS_2 edges as a function of chiral angle χ ($0° \leq \chi \leq 360°$) at various chemical potentials of sulfur μ_s, (a) −2.0 eV (Mo-rich), (b) −1.8 eV (c) −1.4 eV, (d) −1.2 eV, (e) −1 eV, (f) −0.8 eV, (g) −0.6 eV, (h) −0.4 eV, (i) 0 eV, and (j) 0.35 eV (S-rich). The blue, green, and red solid lines denote ZZM, ZZS, and AC edges, respectively. ZZS, S-terminated zigzag edge; ZZM, Mo-terminated zigzag edge; AC, armchair edge. (For interpretation of the references to color in this figure legend, the reader is referred to the Web version of this article.)

between our computational results and experimental observed ones under STEM or in CVD growth [33]. In the current calculation, only the most stable edge structures with global minimum energies are considered to determine the equilibrium shape of monolayer 1H−MoS_2. The equilibrium shape of monolayer 1H−MoS_2 will change in experiments because other experimental factors, such as the temperature, defects, precursor fluxes, electron irradiation, and substrate, will modulate the edges of 1H−MoS_2 to local minima of the potential energy surface [33,57]. These complex experimental environments also provide an opportunity to capture the metastable edge structures such as Mo-Klein edge, DT edge, and Mo-terminated edge (Fig. S7) in experiments. Another possible reason is that, during CVD growth of 1H−MoS_2, the dominating edge is generally the edge grow slowest, determined by the kinetic Wulff construction [58], whereas in the current study, the thermodynamic Wulff construction only predicts the edges with the lowest formation energy. Therefore, the 1H−MoS_2 nanoflakes constructed by our theoretical method could be different from the experimentally observed ones, either under STEM or in CVD growth.

4. Conclusions

In summary, we have systematically explored the possible edge reconstructions of TMDC materials and presented a database of the edge structures of 1H−MoS_2. The potential energy surfaces of three types of 1H−MoS_2 edges, ZZM, ZZS, and AC, are fully explored, and the most stable edges are found to vary with the chemical environment or the chemical potential. Our global search finds 34 highly stable edge structures, and their relative stabilities as a function of chemical potential are calculated. The edge structures predicted in the current calculations match the experimental observations very well. The edge evolution of 1H−MoS_2 nanoflakes and the electronic properties of 1H−MoS_2 nanoribbons are explored. Some unique sulfur-terminated edges with S_2 dimers or sulfur monomers have potential applications as catalysts. In addition to the most stable edge structures, several metastable edge structures with small energy differences with respect to the most stable structure are expected to be synthesized experimentally. This database of edge structures of TMDCs provides not only fundamental information for the study of 1H−MoS_2 edges but also new opportunities in the study of the edge structures of various 2D 1H phase TMDC materials.

Data availability

The raw/processed data required to reproduce these findings cannot be shared at this time as the data also forms part of an ongoing study.

Authors contribution

Ding Feng: Conceptualization, Methodology, Supervision, Writing-Reviewing and Editing. **Li Da:** Methodology, Software, Data curation, Writing-Original draft preparation.

Declaration of Competing Interest

The authors declare that they have no known competing financial interests or personal relationships that could have appeared to influence the work reported in this article.

Acknowledgments

F. D. acknowledges the support from the Institute for Basic Science (IBS-R019-D1) of South Korea and the computational resources from CMCM, IBS. D. L. acknowledges the support from the National Natural Science Foundation of China (91745203, 11404134).

Appendix A. Supplementary data

Supplementary data to this article can be found online at https://doi.org/10.1016/j.mtadv.2020.100079.

References

[1] J. Zhou, J. Lin, X. Huang, Y. Zhou, Y. Chen, J. Xia, H. Wang, Y. Xie, H. Yu, J. Lei, D. Wu, F. Liu, Q. Fu, Q. Zeng, C.-H. Hsu, C. Yang, L. Lu, T. Yu, Z. Shen, H. Lin,

B.I. Yakobson, Q. Liu, K. Suenaga, G. Liu, Z. Liu, A library of atomically thin metal chalcogenides, Nature 556 (2018) 355.
[2] W. Wu, L. Wang, Y. Li, F. Zhang, L. Lin, S. Niu, D. Chenet, X. Zhang, Y. Hao, T.F. Heinz, J. Hone, Z.L. Wang, Piezoelectricity of single-atomic-layer MoS_2 for energy conversion and piezotronics, Nature 514 (2014) 470–474.
[3] M. Chhowalla, H.S. Shin, G. Eda, L.-J. Li, K.P. Loh, H. Zhang, The chemistry of two-dimensional layered transition metal dichalcogenide nanosheets, Nat. Chem. 5 (2013) 263–275.
[4] Y. Yu, G.-H. Nam, Q. He, X.-J. Wu, K. Zhang, Z. Yang, J. Chen, Q. Ma, M. Zhao, Z. Liu, F.-R. Ran, X. Wang, H. Li, X. Huang, B. Li, Q. Xiong, Q. Zhang, Z. Liu, L. Gu, Y. Du, W. Huang, H. Zhang, High phase-purity 1T′-MoS_2- and 1T′-$MoSe_2$-layered crystals, Nat. Chem. 10 (2018) 638.
[5] V. Senthilkumar, L.C. Tam, Y.S. Kim, Y. Sim, M.-J. Seong, J.I. Jang, Direct vapor phase growth process and robust photoluminescence properties of large area MoS_2 layers, Nano Res. 7 (2014) 1759–1768.
[6] J. Kibsgaard, Z. Chen, B.N. Reinecke, T.F. Jaramillo, Engineering the surface structure of MoS_2 to preferentially expose active edge sites for electrocatalysis, Nat. Mater. 11 (2012) 963–969.
[7] T.F. Jaramillo, K.P. Jørgensen, J. Bonde, J.H. Nielsen, S. Horch, I. Chorkendorff, Identification of active edge sites for electrochemical H_2 evolution from MoS_2 nanocatalysts, Science 317 (2007) 100–102.
[8] H.I. Karunadasa, E. Montalvo, Y. Sun, M. Majda, J.R. Long, C.J. Chang, A molecular MoS_2 edge site mimic for catalytic hydrogen generation, Science 335 (2012) 698–702.
[9] P.C.K. Vesborg, B. Seger, I. Chorkendorff, Recent development in hydrogen evolution reaction catalysts and their practical implementation, J. Phys. Chem. Lett. 6 (2015) 951–957.
[10] A.B. Laursen, S. Kegnæs, S. Dahl, I. Chorkendorff, Molybdenum sulfides' efficient and viable materials for electro - and photoelectrocatalytic hydrogen evolution, Energy Environ. Sci. 5 (2012) 5577–5591.
[11] J.V. Lauritsen, J. Kibsgaard, S. Helveg, H. Topsøe, B.S. Clausen, E. Lægsgaard, F. Besenbacher, Size-dependent structure of MoS_2 nanocrystals, Nat. Nanotechnol. 2 (2007) 53–58.
[12] A. Tuxen, J. Kibsgaard, H. Gøbel, E. Lægsgaard, H. Topsøe, J.V. Lauritsen, F. Besenbacher, Size threshold in the dibenzothiophene adsorption on MoS_2 nanoclusters, ACS Nano 4 (2010) 4677–4682.
[13] A. Bruix, H.G. Fu¨chtbauer, A.K. Tuxen, A.S. Walton, M. Andersen, S. Porsgaard, F. Besenbacher, B. Hammer, J.V. Lauritsen, In situ detection of active edge sites in single-layer MoS_2 catalysts, ACS Nano 9 (2015) 9322–9330.
[14] X. Sang, X. Li, W. Zhao, J. Dong, C.M. Rouleau, D.B. Geohegan, F. Ding, K. Xiao, R.R. Unocic, In situ edge engineering in two-dimensional transition metal dichalcogenides, Nat. Commun. 9 (2018) 2051.
[15] M.-R. Gao, M.K.Y. Chan, Y. Sun, Edge-terminated molybdenum disulfide with a 9.4-Å interlayer spacing for electrochemical hydrogen production, Nat. Commun. 6 (2015) 7493.
[16] L.P. Hansen, Q.M. Ramasse, C. Kisielowski, M. Brorson, E. Johnson, H. Topsøe, S. Helveg, Atomic-scale edge structures on industrial-style MoS_2 nanocatalysts, Angew. Chem. Int. Ed. 50 (2011) 10153–10156.
[17] C. Tsai, H. Li, S. Park, J. Park, H.S. Han, J.K. Nørskov, X. Zheng, F. Abild-Pedersen, Electrochemical generation of sulfur vacancies in the basal plane of MoS_2 for hydrogen evolution, Nat. Commun. 8 (2017) 15113.
[18] D.Y. Chung, S.-K. Park, Y.-H. Chung, S.-H. Yu, D.-H. Lim, N. Jung, H.C. Ham, H.-Y. Park, Y. Piao, S.J. Yoo, Y.-E. Sung, Edge-exposed MoS_2 nano-assembled structures as efficient electrocatalysts for hydrogen evolution reaction, Nanoscale 6 (2014) 2131–2136.
[19] X.-L. Fan, Y. Yang, P. Xiao, W.-M. Lau, Site-specific catalytic activity in exfoliated MoS_2 single-layer polytypes for hydrogen evolution: basal plane and edges, J. Mater. Chem. 2 (2014) 20545–20551.
[20] H. Wang, Z. Lu, S. Xu, D. Kong, J.J. Cha, G. Zheng, P.-C. Hsu, K. Yan, D. Bradshaw, F.B. Prinz, Y. Cui, Electrochemical tuning of vertically aligned MoS_2 nanofilms and its application in improving hydrogen evolution reaction, Proc. Natl. Acad. Sci. U. S. A 110 (2013) 19701–19706.
[21] J.D. Benck, Z. Chen, L.Y. Kuritzky, A.J. Forman, T.F. Jaramillo, Amorphous molybdenum sulfide catalysts for electrochemical hydrogen production: insights into the origin of their catalytic activity, ACS Catal. 2 (2012) 1916–1923.
[22] D. Kong, H. Wang, J.J. Cha, M. Pasta, K.J. Koski, J. Yao, Y. Cui, Synthesis of MoS_2 and $MoSe_2$ films with vertically aligned layers, Nano Lett. 13 (2013) 1341–1347.
[23] Y. Yan, B. Xia, X. Ge, Z. Liu, J.-Y. Wang, X. Wang, Ultrathin MoS_2 nanoplates with rich active sites as highly efficient catalyst for hydrogen evolution, ACS Appl. Mater. Interfaces 5 (2013) 12794–12798.
[24] X. Zhang, F. Meng, S. Mao, Q. Ding, M.J. Shearer, M.S. Faber, J. Chen, R.J. Hamers, S. Jin, Amorphous MoS_xCl_y electrocatalyst supported by vertical graphene for efficient electrochemical and photoelectrochemical hydrogen generation, Energy Environ. Sci. 8 (2015) 862–868.
[25] T.A. Ho, C. Bae, S. Lee, M. Kim, J.M. Montero-Moreno, J.H. Park, H. Shin, Edge-on MoS_2 thin films by atomic layer deposition for understanding the interplay between the active area and hydrogen evolution reaction, Chem. Mater. 29 (2017) 7604–7614.
[26] J. Hu, B. Huang, C. Zhang, Z. Wang, Y. An, D. Zhou, H. Lin, M.K.H. Leung, S. Yang, Engineering stepped edge surface structures of MoS_2 sheet stacks to accelerate the hydrogen evolution reaction, Energy Environ. Sci. 10 (2017) 593–603.
[27] Y.-S. Shim, K.C. Kwon, J.M. Suh, K.S. Choi, Y.G. Song, W. Sohn, S. Choi, K. Hong, J.-M. Jeon, S.-P. Hong, S. Kim, S.Y. Kim, C.-Y. Kang, H.W. Jang, Synthesis of numerous edge sites in MoS_2 via SiO_2 nanorods platform for highly sensitive gas sensor, ACS Appl. Mater. Interfaces 10 (2018) 31594–31602.
[28] J. Zhang, J.M. Soon, K.P. Loh, J. Yin, J. Ding, M.B. Sullivian, P. Wu, Magnetic molybdenum disulfide nanosheet films, Nano Lett. 7 (2007) 2370–2376.
[29] X. Zhao, D. Fu, Z. Ding, Y.-Y. Zhang, D. Wan, S.J.R. Tan, Z. Chen, K. Leng, J. Dan, W. Fu, D. Geng, P. Song, Y. Du, T. Venkatesan, S.T. Pantelides, S.J. Pennycook, W. Zhou, K.P. Loh, Mo-terminated edge reconstructions in nanoporous molybdenum disulfide film, Nano Lett. 18 (2018) 482–490.
[30] W. Zhou, X. Zou, S. Najmaei, Z. Liu, Y. Shi, J. Kong, J. Lou, P.M. Ajayan, B.I. Yakobson, J.-C. Idrobo, Intrinsic structural defects in monolayer molybdenum disulfide, Nano Lett. 13 (2013) 2615–2622.
[31] Q. Chen, H. Li, W. Xu, S. Wang, H. Sawada, C.S. Allen, A.I. Kirkland, J.C. Grossman, J.H. Warner, Atomically flat zigzag edges in monolayer MoS_2 by thermal annealing, Nano Lett. 17 (2017) 5502–5507.
[32] H. Xu, S. Liu, Z. Ding, S.J.R. Tan, K.M. Yam, Y. Bao, C.T. Nai, M.-F. Ng, J. Lu, C. Zhang, K.P. Loh, Oscillating edge states in one-dimensional MoS_2 nanowires, Nat. Commun. 7 (2016) 12904.
[33] S. Wang, Y. Rong, Y. Fan, M. Pacios, H. Bhaskaran, K. He, J.H. Warner, Shape evolution of monolayer MoS_2 crystals grown by chemical vapor deposition, Chem. Mater. 26 (2014) 6371–6379.
[34] S.Y. Yang, G.W. Shim, S.-B. Seo, S.-Y. Choi, Effective shape-controlled growth of monolayer MoS_2 flakes by powder-based chemical vapor deposition, Nano Res. 10 (2017) 255–262.
[35] S.S. Grønborg, N. Salazar, A. Bruix, J. Rodríguez-Fernández, S.D. Thomsen, B. Hammer, J.V. Lauritsen, Visualizing hydrogen-induced reshaping and edge activation in MoS_2 and Co-promoted MoS_2 catalyst clusters, Nat. Commun. 9 (2018) 2211.
[36] B. Hinnemann, P.G. Moses, J. Bonde, K.P. Jørgensen, J.H. Nielsen, S. Horch, I. Chorkendorff, J.K. Nørskov, Biomimetic hydrogen evolution: MoS_2 nanoparticles as catalyst for hydrogen evolution, J. Am. Chem. Soc. 127 (2005) 5308–5309.
[37] P. Raybaud, J. Hafner, G. Kresse, S. Kasztelan, H. Toulhoat, Ab initio study of the H_2-H_2S/MoS_2 gas-solid interface: the nature of the catalytically active sites, J. Catal. 189 (2000) 129–146.
[38] D. Cao, T. Shen, P. Liang, X. Chen, H. Shu, Role of chemical potential in flake shape and edge properties of monolayer MoS_2, J. Phys. Chem. C 119 (2015) 4294–4301.
[39] M.C. Lucking, J. Bang, H. Terrones, Y.-Y. Sun, S. Zhang, Multivalency-induced band gap opening at MoS_2 edges, Chem. Mater. 27 (2015) 3326–3331.
[40] J.P. Perdew, K. Burke, M. Ernzerhof, Generalized gradient approximation made simple, Phys. Rev. Lett. 77 (1996) 3865–3868.
[41] G. Kresse, D. Joubert, From ultrasoft pseudopotentials to the projector augmented-wave method, Phys. Rev. B 59 (1999) 1758–1775.
[42] P.E. Blöchl, Projector augmented-wave method, Phys. Rev. B 50 (1994) 17953–17979.
[43] W. Kohn, L.J. Sham, Self-consistent equations including exchange and correlation effects, Phys. Rev. 140 (1965) A1133–A1138.
[44] P. Koskinen, S. Malola, H. Häkkinen, Self-passivating edge reconstructions of graphene, Phys. Rev. Lett. 101 (2008) 115502.
[45] J. Gao, J. Zhao, F. Ding, Transition metal surface passivation induced graphene edge reconstruction, J. Am. Chem. Soc. 134 (2012) 6204–6209.
[46] X. Zhang, J. Xin, F. Ding, The edges of graphene, Nanoscale 5 (2013) 2556–2569.
[47] R. Zhao, J. Gao, Z. Liu, F. Ding, The reconstructed edges of the hexagonal BN, Nanoscale 7 (2015) 9723–9730.
[48] Y. Wang, J. Lv, L. Zhu, Y. Ma, Crystal structure prediction via particle-swarm optimization, Phys. Rev. B 82 (2010), 094116.
[49] Y. Wang, J. Lv, L. Zhu, Y. Ma, CALYPSO: a method for crystal structure prediction, Comput. Phys. Commun. 183 (2012) 2063–2070.
[50] S. Lu, Y. Wang, H. Liu, M.-s. Miao, Y. Ma, Self-assembled ultrathin nanotubes on diamond (100) surface, Nat. Commun. 5 (2014) 3666.
[51] Y. Zhang, W. Wu, Y. Wang, S.A. Yang, Y. Ma, Pressure-stabilized semiconducting electrides in alkaline-earth-metal subnitrides, J. Am. Chem. Soc. 139 (2017) 13798–13803.
[52] P.H. Joo, J. Cheng, K. Yang, Size effects and odd-even effects in MoS_2 nanosheets: first-principles studies, Phys. Chem. Chem. Phys. 19 (2017) 29927–29933.
[53] K. Chen, J. Deng, X. Ding, J. Sun, S. Yang, J.Z. Liu, Ferromagnetism of 1T-MoS_2 nanoribbons stabilized by edge reconstruction and its periodic variation on nanoribbons width, J. Am. Chem. Soc. 140 (2018) 16206–16212.
[54] S. Helveg, J.V. Lauritsen, E. Lægsgaard, I. Stensgaard, J.K. Nørskov, B.S. Clausen, H. Topsøe, F. Besenbacher, Atomic-scale structure of single-layer MoS_2 nanoclusters, Phys. Rev. Lett. 84 (2000) 951–954.
[55] N. Wang, D. Cao, J. Wang, P. Liang, X. Chen, H. Shu, Semiconducting edges and flake-shape evolution of monolayer GaSe: role of edge reconstructions, Nanoscale 10 (2018) 12133–12140.
[56] H. Schweiger, P. Raybaud, G. Kresse, H. Toulhoat, Shape and edge sites modifications of MoS_2 catalytic nanoparticles induced by working conditions: a theoretical study, J. Catal. 207 (2002) 76–87.
[57] K. Momeni, Y. Ji, K. Zhang, J.A. Robinson, L.-Q. Chen, Multiscale framework for simulation-guided growth of 2D materials, npj 2D Mater. Appl. 2 (2018) 27.
[58] J. Dong, L. Zhang, F. Ding, Kinetics of graphene and 2D materials growth, Adv. Mater. 31 (2019) 1801583.